Stability Enhancement of Decentralized Inverter Control through Wireless Communications in Microgrids

Hao Liang, *Student Member, IEEE*, Bong Jun Choi, *Member, IEEE*, Weihua Zhuang, *Fellow, IEEE*, and Xuemin (Sherman) Shen, *Fellow, IEEE*

***Abstract*—Decentralized inverter control is essential in distributed generation (DG) microgrids for low deployment/operation cost and high reliability. However, decentralized inverter control suffers from a limited system stability mainly because of the lack of communications among different inverters. In this paper, we investigate stability enhancement of the droop based decentralized inverter control in microgrids. Specifically, we propose a power sharing based control strategy which incorporates the information of the total real and reactive power generation of all DG units. The information is acquired by a wireless network (such as a WiFi, ZigBee, and/or cellular communication network) in a decentralized manner. Based on the desired power sharing of each DG unit and the acquired information of total generation, additional control terms are added to the traditional droop controller. We evaluate the performance of the proposed control strategy based on small-signal stability analysis. As timely communication may not be established for a microgrid with low-cost wireless communication devices, two kinds of analytical models are developed with respect to negligible and nonnegligible communication delays, respectively. Extensive numerical results are presented to demonstrate the system stability under the proposed control strategy with respect to different communication delays.**

***Index Terms*—Delay, droop control, inverter, microgrid, smart grid, stability, wireless network.**

I. Introduction

Distributed generation (DG) of electricity based on renewable energy sources such as wind and solar is gaining more and more interests all over the world because of ever-growing concerns on energy cost, energy security, and environmental issues. Although DG has a great potential for economic and environmental benefits, how to establish efficient and reliable control over a large number of DG units is one of the primal problems to be solved in the near future. One promising solution to this problem is the microgrid, which interconnects a group of DG units and loads at a distribution voltage level in a local area such as an university or a residential community [1] [2]. Microgrids are established based on localized control and can operate in either a grid-connected mode or an islanded mode, which significantly reduces the complexity of DG unit control. In order to avoid high capital expenditure and low reliability in microgrid operation, decentralized control is indispensable [3].

In this paper, we investigate one of the critical control problems in microgrids, i.e., the droop based decentralized inverter control. The main objective is to achieve efficient real and reactive power sharing while maintaining the microgrid frequency and voltage [4]. Featured by a decentralized control strategy without a communication network infrastructure, the traditional droop control strategy emulates the droop characteristics of synchronous generators based on local estimates on real and reactive power generation. However, in a typical microgrid application where the ratio of line resistance to line reactance is high, the coupling between real and reactive power control deteriorates the system stability [5]. Several methods can be used to improve the stability of traditional droop control in microgrids. For instance, an adaptive transient droop function can be added to damp the oscillatory modes of the power sharing controller [4], while the transient droop gains can be adaptively scheduled based on a small-signal analysis with respect to the loading trajectory of each DG unit. The virtual impedance method can be used to decouple the real and reactive power control [6] [7], especially for the transformer coupled DG units which already have significant output inductance [8]. In order to avoid the complexity in impedance design, the virtual frequency and voltage frame based droop control strategy can be used [9]. The frequency and voltage are transformed to a virtual frame for a completely decoupled relationship between real and reactive power.

In comparison with the existing approaches which improve the traditional droop control strategy of individual inverters, we address the stability enhancement of droop control by establishing coordination among the inverters based on a wireless network. The objective of this research is to introduce limited communication overhead to improve the stability while maintaining the decentralized structure of the traditional droop control strategy. A power sharing based control strategy is proposed based on the information provided by a wireless network, i.e., the total real and reactive power generation of all DG units. The information acquisition is completed in a decentralized manner in accordance with the decentralized inverter control. By evaluating the differences between the desired and actual real and reactive power sharing of each DG unit, additional control terms are incorporated in the traditional droop controller to improve the system stability. Specifically, a proportional term is incorporated in the frequency droop

This work is presented in part in a paper to be presented at IEEE Globecom 2012 [1].

H. Liang, W. Zhuang, and X. Shen are with the Department of Electrical and Computer Engineering, University of Waterloo, 200 University Avenue West, Waterloo, Ontario, Canada N2L 3G1 (e-mail: {h8liang, wzhuang, sshen}@uwaterloo.ca).

B. J. Choi is with the Department of Computer Science, State University of New York Korea, 119 Songdo Moonwhat-Ro, Yeonsu-Gu, Incheon, Korea 406-840 (e-mail: bjchoi@sunykorea.ac.kr).

control to damp the oscillation in real power sharing without affecting the original droop gain. On the other hand, an integral term is incorporated in the voltage droop control to correct the inaccurate reactive power sharing based on the traditional droop control. As timely communication may not be established for a microgrid with a low-cost wireless network infrastructure, the communication delay may adversely affect the performance of microgrid control [2] [10]. Therefore, we extend our previously proposed power sharing based control strategy [1] by considering the impact of communication delay. Analytical models are established to evaluation the stability of microgrids under our proposed control strategy with different communication delay values. To facilitate the analysis, we decompose the small-signal model of the microgrid with respect to the traditional droop control terms and the power sharing based control terms, respectively, and use an approximation algorithm to calculate the modes of the small-signal model. Numerical results indicate that our proposed control strategy can improve system stability as compared with the traditional droop control strategy when the communication delay is small.

The remainder of this paper is organized as follows. Section II describes the system model. Section III presents the proposed power sharing based control strategy. The performance analysis with respect to negligible and nonnegligible communication delays is presented in Section IV and Section V, respectively. Numerical results are presented in Section VI. Section VII concludes this research work.

II. System Model

Consider an islanded microgrid with parallel-connected inverters, as shown in Fig. 1. In the microgrid, there are G inverters (corresponding to the DG units), H loads, N nodes (or connection points), and L power transmission lines. Each line in the microgrid interconnects a pair of two nodes, while each node is connected to an inverter and/or a load. Without loss of generality, we order the elements in the microgrid such that the sets of inverters, loads, nodes, and lines are given by $\{1, 2, \cdots, G\}$, $\{1, 2, \cdots, H\}$, $\{1, 2, \cdots, N\}$, and $\{1, 2, \cdots, L\}$, respectively. A wireless network is established to provide wireless communication links among the inverters. Each inverter is equipped with a wireless communication device which can communicate with a certain set of inverters. The wireless network is considered to be strongly connected, i.e., there exists a communication (possibly multi-hop) path between any pair of two inverters.

The droop based decentralized inverter control strategy is considered [4] [5]. As shown in Fig. 2, the controller of each individual inverter consists of three parts, i.e., the power controller, voltage controller, and current controller. In this work, we consider the stability of power controller, while the voltage and current controllers are based on traditional proportional-integral (PI) controllers. The D-Q reference frame transformation is considered, where the d-axis and q-axis of the reference frame of each inverter are rotating at the reference frequency [11]. Based on the traditional droop control strategy, the reference frequency and output d-axis voltage of inverter g ($g \in \{1, 2, \cdots, G\}$) are determined by the power

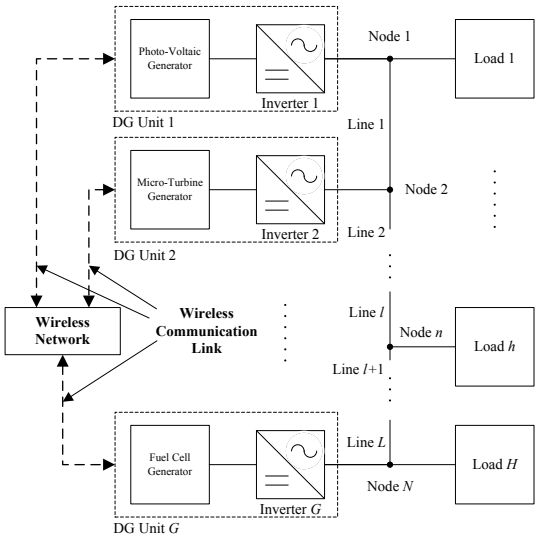

Fig. 1: The configuration of a microgrid with wireless communications among inverters.

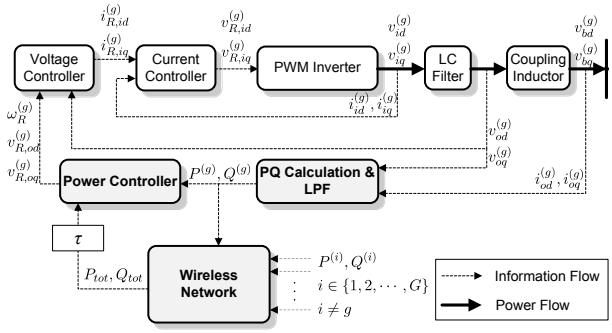

Fig. 2: The block diagram of an inverter controller.

controller and are given by

$$\omega_{R-dr}^{(g)} = \omega_0 - K_{P-dr}^{(g)} P^{(g)} \tag{1}$$

$$v_{R-dr,od}^{(g)} = v_{0,od} - K_{Q-dr}^{(g)} Q^{(g)} \tag{2}$$

$$v_{R-dr,oq}^{(g)} = 0 \tag{3}$$

where ω_0 and $v_{0,od}$ are the nominal set points of frequency and d-axis output voltage, respectively, while $K_{P-dr}^{(g)}$ and $K_{Q-dr}^{(g)}$ are the frequency and voltage droop gains with respect to certain ranges of frequency and voltage magnitude, $[\omega_{\min}^{(g)}, \omega_{\max}^{(g)}]$ and $[v_{\min,od}^{(g)}, v_{\max,od}^{(g)}]$, respectively, given by

$$K_{P-dr}^{(g)} = \frac{\omega_{\max}^{(g)} - \omega_{\min}^{(g)}}{P_{\max}^{(g)}} \tag{4}$$

$$K_{Q-dr}^{(g)} = \frac{v_{\max,od}^{(g)} - v_{\min,od}^{(g)}}{Q_{\max}^{(g)}}. \tag{5}$$

In (1)-(3), we use the subscript "$-dr$" to denote the values determined based on the traditional droop control strategy. Since no communication network is available for traditional droop control, $\omega_{R-dr}^{(g)}$, $v_{R-dr,od}^{(g)}$, and $v_{R-dr,oq}^{(g)}$ are equal to $\omega_R^{(g)}$, $v_{R,od}^{(g)}$, and $v_{R,oq}^{(g)}$ in Fig. 2.

The inputs of the power controller, i.e., the real power ($P^{(g)}$)

and reactive power ($Q^{(g)}$), are calculated based on the low-pass filtered (with cutoff frequency ω_c) values of $p^{(g)}$ and $q^{(g)}$, respectively, given by

$$p^{(g)} = v_{od}^{(g)} i_{od}^{(g)} + v_{oq}^{(g)} i_{oq}^{(g)} \tag{6}$$

$$q^{(g)} = v_{od}^{(g)} i_{oq}^{(g)} - v_{oq}^{(g)} i_{od}^{(g)}. \tag{7}$$

The output $\omega_R^{(g)}$ of the power controller is used by the pulse-width modulation (PWM) inverter as reference frequency, while the reference voltage of the PWM inverter needs to be regulated by the following voltage and current controllers.

Based on the references provided by the power controller, $v_{R,od}^{(g)}$ and $v_{R,oq}^{(g)}$, the output of the voltage controller is given by

$$\begin{aligned} i_{R,id}^{(g)} = {} & K_{pv}[v_{R,od}^{(g)} - v_{od}^{(g)}] + K_{iv}\int [v_{R,od}^{(g)} - v_{od}^{(g)}]dt \\ & - w_0 C_f v_{oq}^{(g)} + F i_{od}^{(g)} \end{aligned} \tag{8}$$

$$\begin{aligned} i_{R,iq}^{(g)} = {} & K_{pv}[v_{R,oq}^{(g)} - v_{oq}^{(g)}] + K_{iv}\int [v_{R,oq}^{(g)} - v_{oq}^{(g)}]dt \\ & + w_0 C_f v_{od}^{(g)} + F i_{oq}^{(g)} \end{aligned} \tag{9}$$

where K_{pv} and K_{iv} are the proportional and integral gains of the voltage controller, respectively, while C_f and F are the capacitance of the LC filter and feedforward gain, respectively. On the other hand, based on the references provided by the voltage controller, $i_{R,id}^{(g)}$ and $i_{R,iq}^{(g)}$, the output of the current controller is given by

$$\begin{aligned} v_{R,id}^{(g)} = {} & K_{pi}[i_{R,id}^{(g)} - i_{id}^{(g)}] + K_{ii}\int [i_{R,id}^{(g)} - i_{id}^{(g)}]dt \\ & - w_0 L_f I_{Iq}^{(g)} \end{aligned} \tag{10}$$

$$\begin{aligned} v_{R,iq}^{(g)} = {} & K_{pi}[i_{R,iq}^{(g)} - i_{iq}^{(g)}] + K_{ii}\int [i_{R,iq}^{(g)} - i_{iq}^{(g)}]dt \\ & + w_0 L_f v_{oq}^{(g)} \end{aligned} \tag{11}$$

where K_{pi} and K_{ii} are the proportional and integral gains of the current controller, respectively, while L_f is the inductance of the LC filter.

The rationale behind the traditional droop control strategy is that the microgrid frequency and voltage can be considered as two virtual communication links among the inverters. However, this kind of virtual communication is effective only when the transmission lines are mainly inductive, based on which the control of real and reactive power generation can be decoupled [9]. For a typical microgrid configuration where the line resistance is significant as compared with line inductance, the real and reactive power control is coupled such that the traditional droop control (with respect to (1)-(3)) deteriorates the system stability.

III. The Power Sharing Based Control Strategy

In order to improve the system stability under decentralized inverter control, we propose a power sharing based control strategy which utilizes the information with respect to the total real power generation ($P_{tot} = \sum_{i=1}^{G} P^{(i)}$) and reactive power generation ($Q_{tot} = \sum_{i=1}^{G} Q^{(i)}$) of all DG units, as shown in Fig. 2. The grey control blocks correspond to the modified blocks as compared with the traditional droop control strategy. Auxiliary control terms are added to the traditional droop controller, which correspond to the differences between desired and actual sharing of real and reactive power of each DG unit. The information is acquired by the wireless network in a decentralized manner.

A. Controller Design

According to the power sharing based control strategy, the reference frequency and voltages of inverter g are, respectively, given by

$$\omega_R^{(g)} = \omega_{R-dr}^{(g)} + K_{P-sh}^{(g)}[\alpha_P^{(g)} P_{tot} - P^{(g)}] \tag{12}$$

$$v_{R,od}^{(g)} = v_{R-dr,od}^{(g)} + K_{Q-sh}^{(g)}\int [\alpha_Q^{(g)} Q_{tot} - Q^{(g)}]dt \tag{13}$$

$$v_{R,oq}^{(g)} = 0 \tag{14}$$

where $K_{P-sh}^{(g)}$ and $K_{Q-sh}^{(g)}$ are the control gains with respect to the real and reactive power sharing, respectively, while $\alpha_P^{(g)}$ and $\alpha_Q^{(g)}$ are the desired sharing of real and reactive power by DG unit g, respectively. Obviously, we have $\sum_{g=1}^{G} \alpha_P^{(g)} = 1$ and $\sum_{g=1}^{G} \alpha_Q^{(g)} = 1$.

The rationale behind the controller is to use the actual sharing of real and reactive power to fine tune the reference frequency and voltage of each inverter. With a larger difference, the frequency (or voltage) reference of an individual inverter is adjusted more significantly, and vice versa. The adjustment is stopped when the desired sharing is achieved. Note that an integral term is used for the voltage reference since the reactive power sharing of a tradition droop controller is inaccurate for microgrid applications [12]. It is worth mentioning that our proposed control strategy reduces to the traditional droop control strategy by letting $K_{P-sh}^{(g)} = 0$ and $K_{Q-sh}^{(g)} = 0$.

B. Decentralized Information Acquisition

The information acquisition is carried out based on the wireless network in a decentralized manner. Here, we consider a multiagent coordination based decentralized information acquisition scheme which can be applied to wireless networks[1] such as WiFi, ZigBee, and cellular communication networks [10] [15]. The communication is fully decentralized such that each inverter only needs to communicate with its direct neighbors to calculate the total generation of all DG units in the microgrid (i.e., P_{tot} and Q_{tot}). The convergence of the information acquisition is guaranteed based on the average consensus theory [16] [17] [18]. We omit the details of the communication protocol design here because of the space limitation. However, in achieving convergence among the multiagent coordination results with certain accuracy, we need to take into account that a communication delay τ may exist as shown in Fig. 2, which corresponds to the period between the information (i.e., $P^{(i)}$ and $Q^{(i)}$ for $i \in \{1, 2, \cdots, G\}$) measurement and the control decision making[2].

[1] An extension of the multiagent coordination scheme to wireline (or power line) communication networks is straightforward [13] [14].

[2] The clock synchronization in microgrids can also be done in a decentralized manner [18], which is out of the scope of this paper.

The delay τ depends on the wireless network. If a long-range low-delay wireless network such as a cellular communication network is available, the communication delay is negligible. The reference frequency and voltage provided by the proposed control strategy are given by (12)-(14). On the other hand, for most of the microgrids where operation cost is one of the major concerns, relying on a high-performance network infrastructure is impractical [4]. Alternatively, low-cost wireless communication devices such as WiFi and ZigBee devices can be used to establish the network infrastructure [3]. For these types of low-cost wireless networks, the communication delay is nonnegligible[3] ($\tau > 0$) in obtaining accurate information acquired by each inverter. The reference frequency and voltage are given by

$$\omega_R^{(g)} = K_{P-sh}^{(g)}[\alpha_P^{(g)} P_{tot}(t-\tau) - P^{(g)}(t-\tau)] + \omega_{R-dr}^{(g)}(t) \tag{15}$$

$$v_{R,od}^{(g)} = K_{Q-sh}^{(g)} \int [\alpha_Q^{(g)} Q_{tot}(t-\tau) - Q^{(g)}(t-\tau)]dt + v_{R-dr,od}^{(g)}(t) \tag{16}$$

$$v_{R,oq}^{(g)} = 0 \tag{17}$$

where $\omega_{R-dr}^{(g)}(t)$ and $v_{R-dr,od}^{(g)}(t)$ are given by (1) and (2), respectively, at time t. Since the communication delay may adversely affect the system stability under our proposed control strategy, we will establish analytical models in the following two sections for performance evaluation with respect to negligible and nonnegligible communication delays, respectively.

IV. Stability Analysis for Negligible Communication Delay

In this section, we present a small-signal model for the performance evaluation of our proposed control strategy. The small-signal model is obtained by linearizing the system state equations at certain operation point. The model can effectively characterize the system stability subject to small disturbances such as load changes (in contrast to large disturbances such as fault and loss of generation) [19], and is widely used to evaluate the stability of decentralized inverter control. In comparison with the small-signal models of traditional droop control strategy, new system states are included in the power controller model since an auxiliary integral term is used for voltage reference calculation. Moreover, in order to capture the effect of introducing a wireless network, the coupling relation among the inverters is established.

In the following analysis, we first establish the model of individual inverter by incorporating new system states and power sharing information. The model is further decomposed into two components in the analysis of combined inverters and microgrid, corresponding to the traditional droop control term (with new system states) and power sharing control term, respectively. The purpose of the decomposition is to separate the model based on the information obtained from the wireless network from that based on the local information of each inverter, and to facilitate the stability analysis for nonnegligible communication delay, to be discussed in Section V.

[3]The delay can be potentially reduced by selectively introducing additional long-range communication links such as cellular communication links, at an extra monetary cost [10].

A. Model of Individual Inverter

In this subsection, the small-signal model for a single inverter is devised. Our focus is on a model for the power controller, while the models of voltage controller, current controller, LC filter, coupling inductance, and output on common reference frame follow the models of traditional droop controller [4] [5].

1) Power Controller: Our proposed power controller incorporates the total real and reactive power generation information of all DG units (i.e., P_{tot} and Q_{tot}). The small-signal state equations of the power controller are given by

$$\Delta\dot{\delta}^{(g)} = \left[-K_{P-dr}^{(g)} + K_{P-sh}^{(g)}\alpha_P^{(g)} - K_{P-sh}^{(g)}\right]\Delta P^{(g)} + \sum_{\substack{i=1\\ i\neq g}}^{G}\left[K_{P-sh}^{(g)}\alpha_P^{(g)}\Delta P^{(i)}\right] - \Delta\omega_{com} \tag{18}$$

$$\Delta\dot{P}^{(g)} = -\omega_c\Delta P^{(g)} + \omega_c I_{od}^{(g)}\Delta v_{od}^{(g)} + \omega_c I_{oq}^{(g)}\Delta v_{oq}^{(g)} + \omega_c V_{od}^{(g)}\Delta i_{od}^{(g)} + \omega_c V_{oq}^{(g)}\Delta i_{oq}^{(g)} \tag{19}$$

$$\Delta\dot{Q}^{(g)} = -\omega_c\Delta Q^{(g)} + \omega_c I_{oq}^{(g)}\Delta v_{od}^{(g)} - \omega_c I_{od}^{(g)}\Delta v_{oq}^{(g)} - \omega_c V_{oq}^{(g)}\Delta i_{od}^{(g)} + \omega_c V_{od}^{(g)}\Delta i_{oq}^{(g)} \tag{20}$$

where $I_{od}^{(g)}$, $I_{oq}^{(g)}$, $V_{od}^{(g)}$, and $V_{oq}^{(g)}$ are the initial values of the inverter output current and voltage, respectively.

Denote $S_Q^{(g)}$ as integrator state of the power controller, which is a new system state we introduced for each inverter in comparison with the model of traditional droop controller. Then, the small-signal model of the integrator is given by

$$\Delta\dot{S}_Q^{(g)} = \alpha_Q^{(g)}\sum_{i=1}^{G}\Delta Q^{(i)} - \Delta Q^{(g)} = \left[\alpha_Q^{(g)} - 1\right]\Delta Q^{(g)} + \alpha_Q^{(g)}\sum_{\substack{i=1\\ i\neq g}}^{G}\Delta Q^{(i)}. \tag{21}$$

The small-signal model with respect to the output reference voltage of the power controller is given by

$$\Delta v_{R,od}^{(g)} = -K_{Q-dr}^{(g)}\Delta Q^{(g)} + K_{Q-sh}^{(g)}\Delta S_Q^{(g)} \tag{22}$$

$$\Delta v_{R,oq}^{(g)} = 0. \tag{23}$$

For the inverter, inverter g, whose reference frame is selected as the common reference frame, there is one more small-signal model with respect to the common reference frequency. Since $\Delta\omega_{com} = \Delta\omega_R^{(g)}$ for the specific inverter, we have

$$\Delta\omega_{com} = \left[-K_{P-dr}^{(g)} + K_{P-sh}^{(g)}\alpha_P^{(g)} - K_{P-sh}^{(g)}\right]\Delta P^{(g)} + \sum_{\substack{i=1\\ i\neq g}}^{G}\left[K_{P-sh}^{(g)}\alpha_P^{(g)}\Delta P^{(i)}\right]. \tag{24}$$

2) Voltage Controller, Current Controller, LC Filter, Coupling Inductance, and Output on Common Reference Frame: Since traditional PI controllers are used for both voltage and

current controllers, additional states $[S_{V,d}^{(g)}\ S_{V,q}^{(g)}]$ and $[S_{I,d}^{(g)}\ S_{I,d}^{(g)}]$ are defined for the integrators of the voltage and current controllers, respectively. Moreover, in order to connect each inverter to the system, the output current and voltage should be converted with respect to the common reference frame. Let the output current of inverter g on the common reference frame be $i_{oDQ}^{(g)} = [i_{oD}^{(g)}\ i_{oQ}^{(g)}]^T$, and denote the bus voltage of node n on the common reference frame as $v_{oDQ}^{(n)} = [v_{bD}^{(n)}\ v_{bQ}^{(n)}]^T$. The small-signal models are given in [5].

3) Small-Signal Model of Individual Inverter: For inverter g, denote the state space of the small-signal model as $\Delta x^{(g)}$, which includes the state spaces of the power controller, voltage controller, current controller, LCL filter, and coupling inductance, given by a 14-element vector

$$\begin{aligned}\Delta x^{(g)} = \Big[&\Delta\delta^{(g)}\ \Delta P^{(g)}\ \Delta Q^{(g)}\ \Delta S_Q^{(g)}\ \Delta S_{V,d}^{(g)}\ \Delta S_{V,q}^{(g)}\\ &\Delta S_{I,d}^{(g)}\ \Delta S_{I,q}^{(g)}\ \Delta i_{id}^{(g)}\ \Delta i_{iq}^{(g)}\ \Delta v_{od}^{(g)}\ \Delta v_{oq}^{(g)}\\ &\Delta i_{od}^{(g)}\ \Delta i_{oq}^{(g)}\Big]^T. \end{aligned} \tag{25}$$

In addition to state $\Delta x^{(g)}$, the small-signal model of inverter g has inputs $\Delta P^{(i)}$ $(i \in \{1,2,\cdots,G\}, i \neq g)$, $\Delta Q^{(i)}$ $(i \in \{1,2,\cdots,G\}, i \neq g)$, $\Delta v_{bDQ}^{(n)} = \left[\Delta v_{bD}^{(n)}, \Delta v_{bQ}^{(n)}\right]^T$, and $\Delta\omega_{com}$. Then, the small-signal model of inverter g is given by

$$\begin{aligned}\Delta\dot{x}^{(g)} = &A_1^{(g)}\Delta x^{(g)} + B_1^{(g)}\Delta v_{bDQ}^{(n)} + B_{com}^{(g)}\Delta\omega_{com}\\ &+ \sum_{i=1}^{G} B_{P,i}^{(g)}\Delta x^{(i)} + \sum_{i=1}^{G} B_{Q,i}^{(g)}\Delta x^{(i)}\end{aligned} \tag{26}$$

where matrix $A_1^{(g)}$ is defined with respect to the state variables, given by

$$A_1^{(g)} = \left[A_{11}^{(g)}\ A_{12}^{(g)}\right]_{14\times 14} \tag{27}$$

and $A_{11}^{(g)}$ and $A_{12}^{(g)}$ are given on the next page. The matrices $B_1^{(g)}$, $B_{com}^{(g)}$, $B_{P,i}^{(g)}$, and $B_{Q,i}^{(g)}$ are defined with respect to the inputs. We have

$$B_1^{(g)} = \begin{bmatrix} 0 & 0\\ \vdots & \vdots\\ 0 & 0\\ -\dfrac{\cos\left(\delta_0^{(g)}\right)}{L_c} & -\dfrac{\sin\left(\delta_0^{(g)}\right)}{L_c}\\ \dfrac{\sin\left(\delta_0^{(g)}\right)}{L_c} & -\dfrac{\cos\left(\delta_0^{(g)}\right)}{L_c}\end{bmatrix}_{14\times 2} \tag{28}$$

$$B_{com}^{(g)} = [-1\ 0\ \cdots\ 0]_{1\times 14}^T. \tag{29}$$

Letting $B_{Q,i}^{(g)} = [b_{Q,i}^{(g)}(j,k)]_{14\times 14}$, we have

$$b_{Q,i=g}^{(g)}(j,k) = \begin{cases}\alpha_Q^{(g)} - 1, & \text{if } j=4 \text{ and } k=3\\ 0, & \text{otherwise}\end{cases} \tag{30}$$

$$b_{Q,i\neq g}^{(g)}(j,k) = \begin{cases}\alpha_Q^{(g)}, & \text{if } j=4 \text{ and } k=3\\ 0, & \text{otherwise.}\end{cases} \tag{31}$$

Denote $B_{P,i}^{(g)}$ as $[b_{P,i}^{(g)}(j,k)]_{14\times 14}$. We have

$$\begin{aligned}&b_{P,i=g}^{(g)}(j,k)\\ &= \begin{cases}K_{P-sh}^{(g)}\alpha_P^{(g)} - K_{P-sh}^{(g)}, & \text{if } j=1, k=2\\ I_{iq}^{(g)}[K_{P-sh}^{(g)}\alpha_P^{(g)} - K_{P-sh}^{(g)}], & \text{if } j=9, k=2\\ -I_{id}^{(g)}[K_{P-sh}^{(g)}\alpha_P^{(g)} - K_{P-sh}^{(g)}], & \text{if } j=10, k=2\\ V_{oq}^{(g)}[K_{P-sh}^{(g)}\alpha_P^{(g)} - K_{P-sh}^{(g)}], & \text{if } j=11, k=2\\ -V_{od}^{(g)}[K_{P-sh}^{(g)}\alpha_P^{(g)} - K_{P-sh}^{(g)}], & \text{if } j=12, k=2\\ I_{oq}^{(g)}[K_{P-sh}^{(g)}\alpha_P^{(g)} - K_{P-sh}^{(g)}], & \text{if } j=13, k=2\\ -I_{od}^{(g)}[K_{P-sh}^{(g)}\alpha_P^{(g)} - K_{P-sh}^{(g)}], & \text{if } j=14, k=2\\ 0, & \text{otherwise}\end{cases}\end{aligned} \tag{32}$$

$$b_{P,i\neq g}^{(g)}(j,k) = \begin{cases}K_{P-sh}^{(g)}\alpha_P^{(g)}, & \text{if } j=1, k=2\\ I_{iq}^{(g)}K_{P-sh}^{(g)}\alpha_P^{(g)}, & \text{if } j=9, k=2\\ -I_{id}^{(g)}K_{P-sh}^{(g)}\alpha_P^{(g)}, & \text{if } j=10, k=2\\ V_{oq}^{(g)}K_{P-sh}^{(g)}\alpha_P^{(g)}, & \text{if } j=11, k=2\\ -V_{od}^{(g)}K_{P-sh}^{(g)}\alpha_P^{(g)}, & \text{if } j=12, k=2\\ I_{oq}^{(g)}K_{P-sh}^{(g)}\alpha_P^{(g)}, & \text{if } j=13, k=2\\ -I_{od}^{(g)}K_{P-sh}^{(g)}\alpha_P^{(g)}, & \text{if } j=14, k=2\\ 0, & \text{otherwise.}\end{cases} \tag{33}$$

By converting the output current of inverter g to the common reference frame, we have

$$\begin{aligned}&\Delta i_{oDQ}^{(g)} = [C_1^{(g)}]^T\Delta x^{(g)}\\ &C_1^{(g)} = \begin{bmatrix}\left[-I_{od}^{(g)}\sin\left(\delta_0^{(g)}\right) & \left[-I_{od}^{(g)}\sin\left(\delta_0^{(g)}\right)\right.\right.\\ \left.\left.-I_{oq}^{(g)}\cos\left(\delta_0^{(g)}\right)\right] & \left.-I_{oq}^{(g)}\cos\left(\delta_0^{(g)}\right)\right]\\ 0 & 0\\ \vdots & \vdots\\ 0 & 0\\ \cos\left(\delta_0^{(g)}\right) & -\sin\left(\delta_0^{(g)}\right)\\ \sin\left(\delta_0^{(g)}\right) & \cos\left(\delta_0^{(g)}\right)\end{bmatrix}_{14\times 2.}\end{aligned} \tag{34}$$

Without loss of generality, select the reference frame of inverter 1 as the common reference frame. Taking account of (24), the small-signal model of the common reference frame is given by

$$\Delta\omega_{com} = C_{com,0}\Delta x^{(1)} + \sum_{i=1}^{G} C_{com,i}\Delta x^{(i)} \tag{35}$$

$$C_{com,i} = \begin{cases}-K_{P-dr}^{(1)}e_2^T, & \text{if } i=0\\ \left[K_{P-sh}^{(1)}\alpha_P^{(1)} - K_{P-sh}^{(1)}\right]e_2^T, & \text{if } i=1\\ K_{P-sh}^{(1)}\alpha_P^{(1)}e_2^T, & \text{otherwise}\end{cases} \tag{36}$$

where e_g is the gth unit vector (of size 14), with the gth element being 1 and all other elements being zero.

B. Combined Inverter Model

Since the information of total generation (P_{tot} and Q_{tot}) is used by each individual inverter, the correlation among different inverters should be considered in the combined

inverter model. The states of all inverters are given by

$$\Delta\mathbf{x} = [\Delta x^{(1)}\ \Delta x^{(2)}\ \cdots\ \Delta x^{(G)}]^T. \tag{37}$$

Denote the states of all bus voltage and generator output current as $\Delta\mathbf{v}_{bDQ}$ and $\Delta\mathbf{i}_{oDQ}$, respectively, given by

$$\begin{aligned}\Delta\mathbf{v}_{bDQ} &= [\Delta v_{bDQ}^{(1)}\ \Delta v_{bDQ}^{(2)}\ \cdots\ \Delta v_{bDQ}^{(N)}]^T\\ \Delta\mathbf{i}_{oDQ} &= [\Delta i_{oDQ}^{(1)}\ \Delta i_{oDQ}^{(2)}\ \cdots\ \Delta i_{oDQ}^{(G)}]^T.\end{aligned} \tag{38}$$

Then, the small-signal model of all inverters is given by

$$\Delta\dot{\mathbf{x}} = \mathbf{A}_1\Delta\mathbf{x} + \mathbf{B}_1\mathbf{M}_1'\Delta\mathbf{v}_{bDQ} \tag{39}$$

$$\Delta\mathbf{i}_{oDQ} = \mathbf{C}_1\Delta\mathbf{x} \tag{40}$$

$$\Delta\omega_{com} = \mathbf{C}_{com}\Delta\mathbf{x}. \tag{41}$$

In (39), matrix $\mathbf{A}_1$ can be decomposed into two components $\mathbf{A}_{1-dr}$ and $\mathbf{A}_{1-sh}$ ($\mathbf{A}_1 = \mathbf{A}_{1-dr} + \mathbf{A}_{1-sh}$), corresponding to the traditional droop control term and power sharing based control term, respectively, where

$$\mathbf{A}_{1-dr} = \begin{bmatrix} \left[A^{(1)} + B_{com}^{(1)}C_{com,0}\right] & 0 & \cdots & 0 \\ \left[B_{com}^{(2)}C_{com,0}\right] & A^{(2)} & \cdots & 0 \\ \vdots & \vdots & \ddots & \vdots \\ \left[B_{com}^{(G)}C_{com,0}\right] & 0 & \cdots & A^{(G)} \end{bmatrix} \tag{42}$$

and the value of $\mathbf{A}_{1-sh}$ is given at the bottom of this page. Similarly, $\mathbf{C}_{com}$ in (41) can be decomposed into two components $\mathbf{C}_{com-dr}$ and $\mathbf{C}_{com-sh}$ ($\mathbf{C}_{com} = \mathbf{C}_{com-dr} + \mathbf{C}_{com-sh}$).

$$A_{11}^{(g)} = \begin{bmatrix} 0 & -K_{P-dr}^{(g)} & 0 & 0 & 0 & 0 \\ 0 & -\omega_c & 0 & 0 & 0 & 0 \\ 0 & 0 & -\omega_c & 0 & 0 & 0 \\ 0 & 0 & 0 & 0 & 0 & 0 \\ 0 & 0 & -K_{Q-dr}^{(g)} & K_{Q-sh}^{(g)} & 0 & 0 \\ 0 & 0 & 0 & 0 & 0 & 0 \\ 0 & 0 & -K_{pv}K_{Q-dr}^{(g)} & K_{pv}K_{Q-sh}^{(g)} & K_{iv} & 0 \\ 0 & 0 & 0 & 0 & 0 & K_{iv} \\ 0 & -K_{P-dr}^{(g)}I_{iq}^{(g)} & \dfrac{-K_{Q-dr}^{(g)}K_{pv}K_{pi}}{L_f} & \dfrac{K_{Q-sh}^{(g)}K_{pv}K_{pi}}{L_f} & \dfrac{K_{pi}K_{iv}}{L_f} & 0 \\ 0 & K_{P-dr}^{(g)}I_{id}^{(g)} & 0 & 0 & 0 & \dfrac{K_{pi}K_{iv}}{L_f} \\ 0 & -K_{P-dr}^{(g)}V_{oq}^{(g)} & 0 & 0 & 0 & 0 \\ 0 & K_{P-dr}^{(g)}V_{od}^{(g)} & 0 & 0 & 0 & 0 \\ -\dfrac{-V_{bD}^{(n)}\sin\left(\delta_0^{(g)}\right) + V_{bQ}^{(n)}\cos\left(\delta_0^{(g)}\right)}{L^c} & -K_{P-dr}^{(g)}I_{oq}^{(g)} & 0 & 0 & 0 & 0 \\ -\dfrac{-V_{bD}^{(n)}\cos\left(\delta_0^{(g)}\right) - V_{bQ}^{(n)}\sin\left(\delta_0^{(g)}\right)}{L_c} & K_{P-dr}^{(g)}I_{od}^{(g)} & 0 & 0 & 0 & 0 \end{bmatrix}_{14\times 6}$$

$$A_{12}^{(g)} = \begin{bmatrix} 0 & 0 & 0 & 0 & 0 & 0 & 0 & 0 \\ 0 & 0 & 0 & 0 & \omega_c I_{od}^{(g)} & \omega_c I_{oq}^{(g)} & \omega_c V_{od}^{(g)} & \omega_c V_{oq}^{(g)} \\ 0 & 0 & 0 & 0 & \omega_c I_{oq}^{(g)} & -\omega_c I_{od}^{(g)} & -\omega_c V_{oq}^{(g)} & \omega_c V_{od}^{(g)} \\ 0 & 0 & 0 & 0 & 0 & 0 & 0 & 0 \\ 0 & 0 & 0 & 0 & -1 & 0 & 0 & 0 \\ 0 & 0 & 0 & 0 & 0 & -1 & 0 & 0 \\ 0 & 0 & -1 & 0 & -K_{pv} & -\omega_0 C_f & F & 0 \\ \dfrac{K_{ii}}{L_f} & 0 & 0 & -1 & \omega_0 C_f & -K_{pv} & 0 & F \\ -\dfrac{R_f + K_{pi}}{L_f} & \omega_{sys} - \omega_0 & -\dfrac{1 + K_{pi}K_{pv}}{L_f} & \dfrac{-\omega_0 C_f K_{pi}}{L_f} & \dfrac{FK_{pi}}{L_f} & 0 & & \\ 0 & \dfrac{K_{ii}}{L_f} & \omega_0 - \omega_{sys} & -\dfrac{R_f + K_{pi}}{L_f} & \dfrac{\omega_0 C_f K_{pi}}{L_f} & -\dfrac{1 + K_{pi}K_{pv}}{L_f} & 0 & \dfrac{FK_{pi}}{L_f} \\ 0 & 0 & \dfrac{1}{C_f} & 0 & 0 & \omega_{sys} & -\dfrac{1}{C_f} & 0 \\ 0 & 0 & 0 & \dfrac{1}{C_f} & -\omega_{sys} & 0 & 0 & -\dfrac{1}{C_f} \\ 0 & 0 & 0 & 0 & \dfrac{1}{L_c} & 0 & -\dfrac{R_c}{L_c} & \omega_{sys} \\ 0 & 0 & 0 & 0 & 0 & \dfrac{1}{L_c} & -\omega_{sys} & -\dfrac{R_c}{L_c} \end{bmatrix}_{14\times 8}$$

$$\mathbf{A}_{1-sh} = \begin{bmatrix} \left[B_{com}^{(1)}C_{com,1} + B_{P,1}^{(1)} + B_{Q,1}^{(1)}\right] & \left[B_{com}^{(1)}C_{com,2} + B_{P,2}^{(1)} + B_{Q,2}^{(1)}\right] & \cdots & \left[B_{com}^{(1)}C_{com,G} + B_{P,G}^{(1)} + B_{Q,G}^{(1)}\right] \\ \left[B_{com}^{(2)}C_{com,1} + B_{P,1}^{(2)} + B_{Q,1}^{(2)}\right] & \left[B_{com}^{(2)}C_{com,2} + B_{P,2}^{(2)} + B_{Q,2}^{(2)}\right] & \cdots & \left[B_{com}^{(2)}C_{com,G} + B_{P,G}^{(2)} + B_{Q,G}^{(2)}\right] \\ \vdots & \vdots & \ddots & \vdots \\ \left[B_{com}^{(G)}C_{com,1} + B_{P,1}^{(G)} + B_{Q,1}^{(G)}\right] & \left[B_{com}^{(G)}C_{com,2} + B_{P,2}^{(G)} + B_{Q,2}^{(G)}\right] & \cdots & \left[B_{com}^{(G)}C_{com,G} + B_{P,G}^{(G)} + B_{Q,G}^{(G)}\right] \end{bmatrix}$$

Based on (35) and (36), we have

$$\mathbf{C}_{com-sh} = [C_{com,0}\ 0\ \cdots\ 0]_{1\times 14G} \tag{43}$$

$$\mathbf{C}_{com-dr} = [C_{com,1}\ C_{com,2}\ \cdots\ C_{com,G}]_{1\times 14G}. \tag{44}$$

In (39), $\mathbf{M}_1' = [m_1'(i,j)]_{2G\times 2N}$ is a matrix which maps the nodes to the inverters. If inverter g is connected to node n, we have $m_1'(2g-1, 2n-1) = m_1'(2g, 2n) = 1$, and 0 otherwise. The matrices $\mathbf{B}_1$ and $\mathbf{C}_1$ are given by

$$\mathbf{B}_1 = \begin{bmatrix} B_1^{(1)} & 0 & \cdots & 0 \\ 0 & B_1^{(2)} & \cdots & 0 \\ \vdots & \vdots & \ddots & \vdots \\ 0 & 0 & \cdots & B_1^{(G)} \end{bmatrix} \tag{45}$$

$$\mathbf{C}_1 = \begin{bmatrix} [C_1^{(1)}]^T & 0 & \cdots & 0 \\ 0 & [C_1^{(2)}]^T & \cdots & 0 \\ \vdots & \vdots & \ddots & \vdots \\ 0 & 0 & \cdots & [C_1^{(G)}]^T \end{bmatrix}. \tag{46}$$

C. Network Model

The network model specifies how the lines and loads are connected to the nodes in the microgrid. We consider the standard model in this work [5]. Denote the state variable for all lines by

$$\Delta\mathbf{i}_{2DQ} = [\Delta i_{2DQ}^{(1)}\ \Delta i_{2DQ}^{(2)}\ \cdots\ \Delta i_{2DQ}^{(L)}]^T \tag{47}$$

where $\Delta i_{2DQ}^{(l)} = [\Delta i_{2D}^{(l)}\ \Delta i_{2Q}^{(l)}]^T$ is the state variable of line l. Then, the small-signal model of the network is given by

$$\Delta\dot{\mathbf{i}}_{2DQ} = \mathbf{A}_2\Delta\mathbf{i}_{2DQ} + \mathbf{B}_{2v}\Delta\mathbf{v}_{bDQ} + \mathbf{B}_{2\omega}\Delta\omega_{com} \tag{48}$$

where the matrices $\mathbf{A}_2$, $\mathbf{B}_{2v}$, and $\mathbf{B}_{2\omega}$ are defined for the output current, bus voltage, and common reference frame, respectively, given at the bottom of this page. The matrix $B_{2v}^{(l)} = [b_{2v}^{(l)}(i,j)]_{2\times 2N}$, which is incorporated in $\mathbf{B}_{2v}$, is given by

$$b_{2v}^{(l)}(i,j) = \begin{cases} 1/L_{line}^{(l)}, & \text{if } (i,j) = (1, 2n_1 - 1) \\ & \text{or } (2, 2n_1) \\ -1/L_{line}^{(l)}, & \text{if } (i,j) = (1, 2n_2 - 1) \\ & \text{or } (2, 2n_2) \\ 0, & \text{otherwise} \end{cases} \tag{49}$$

where n_1 and n_2 are indices (in $\{1, 2, \cdots, N\}$) of the two nodes which are connected by line l, respectively.

Similarly, we can define the load model. Denote the states of the (RL) loads in the microgrid as

$$\Delta\mathbf{i}_{3DQ} = [\Delta i_{3DQ}^{(1)}\ \Delta i_{3DQ}^{(2)}\ \cdots\ \Delta i_{3DQ}^{(H)}]^T \tag{50}$$

where $\Delta i_3^{(h)} = [\Delta i_{3D}^{(h)}\ \Delta i_{3Q}^{(h)}]^T$ is the state of the small-signal model of load h. Then, the small-signal model of all loads in the microgrid is given by

$$\Delta\dot{\mathbf{i}}_{3DQ} = \mathbf{A}_3\Delta\mathbf{i}_{3DQ} + \mathbf{B}_{3v}\Delta\mathbf{v}_{bDQ} + \mathbf{B}_{3\omega}\Delta\omega_{com} \tag{51}$$

where matrices $\mathbf{A}_3$, $\mathbf{B}_{3v}$, and $\mathbf{B}_{3\omega}$ are given at the bottom of this page. The matrix $B_{3v}^{(h)} = [b_{3v}^{(h)}(i,j)]_{2\times 2N}$ in $\mathbf{B}_{3v}$ is given by

$$b_{3v}^{(h)}(i,j) = \begin{cases} 1/L_{load}^{(h)}, & \text{if } (i,j) = (1, 2n-1) \\ & \text{or } (2, 2n) \\ 0, & \text{otherwise} \end{cases} \tag{52}$$

where n is the index of the node connecting to load h.

Let R_N be a sufficiently large (virtual) resistance which connects each node to the ground. Then, the relations among the node voltages can be represented by the currents of the inverters, loads, and transmission lines, given by

$$\Delta\mathbf{v}_{bDQ} = R_N\left(\mathbf{M}_1\mathbf{i}_{oDQ} + \mathbf{M}_2\mathbf{i}_{2DQ} + \mathbf{M}_3\mathbf{i}_{3DQ}\right) \tag{53}$$

where $\mathbf{M}_1 = [m_1(i,j)]_{2N\times 2G}$ is a matrix which maps the inverters to the nodes. If inverter g is connected to node n, we have $m_1(2n-1, 2g-1) = m_1(2n, 2g) = 1$ and 0 otherwise. Similarly, denoting $\mathbf{M}_2 = [m_2(i,j)]_{2N\times 2L}$ and $\mathbf{M}_3 = [m_3(i,j)]_{2N\times 2H}$ for the lines and loads, we have $m_2(2n-1, 2l-1) = m_2(2n, 2l) = 1$ and $m_2(2n-1, 2l-1) = m_2(2n, 2l) = -1$ if line l is entering and leaving the node n, respectively, while $m_3(2n-1, 2h-1) = m_3(2n, 2h) = -1$ if the load h is connected to node n, and 0 otherwise.

D. Microgrid Model

The small-signal model of the entire microgrid is given by

$$\begin{bmatrix} \dot{\Delta\mathbf{x}} \\ \Delta\dot{\mathbf{i}}_{2DQ} \\ \Delta\dot{\mathbf{i}}_{3DQ} \end{bmatrix} = \mathbf{A}_{grid}\begin{bmatrix} \Delta\mathbf{x} \\ \Delta\mathbf{i}_{2DQ} \\ \Delta\mathbf{i}_{3DQ} \end{bmatrix} \tag{54}$$

where $\mathbf{A}_{grid}$ can be decomposed into two components $\mathbf{A}_{grid-dr}$ and $\mathbf{A}_{grid-sh}$ ($\mathbf{A}_{grid} = \mathbf{A}_{grid-dr} + \mathbf{A}_{grid-sh}$) with respect to the traditional droop control term and power sharing based control term, respectively, given at the bottom of the next page, while $\mathbf{R}_N$ is a $2N \times 2N$ diagonal matrix with all diagonal elements equal to R_N. Obviously, the size of $\mathbf{A}_{grid}$ is $(14G + 2L + 2H) \times (14G + 2L + 2H)$.

$$\mathbf{A}_2 = \begin{bmatrix} A_2^{(1)} & 0 & \cdots & 0 \\ 0 & A_2^{(2)} & \cdots & 0 \\ \vdots & \vdots & \ddots & \vdots \\ 0 & 0 & \cdots & A_2^{(L)} \end{bmatrix} \quad \mathbf{B}_{2v} = \begin{bmatrix} B_{2v}^{(1)} \\ B_{2v}^{(2)} \\ \vdots \\ B_{2v}^{(L)} \end{bmatrix} \quad \mathbf{B}_{2\omega} = \begin{bmatrix} B_{2\omega}^{(1)} \\ B_{2\omega}^{(2)} \\ \vdots \\ B_{2\omega}^{(L)} \end{bmatrix} \quad A_2^{(l)} = \begin{bmatrix} -R_{line}^{(l)}/L_{line}^{(l)} & \omega_{sys} \\ -\omega_{sys} & -R_{line}^{(l)}/L_{line}^{(l)} \end{bmatrix} \quad B_{2\omega}^{(l)} = \begin{bmatrix} I_{2Q}^{(l)} \\ -I_{2D}^{(l)} \end{bmatrix}$$

$$\mathbf{A}_3 = \begin{bmatrix} A_3^{(1)} & 0 & \cdots & 0 \\ 0 & A_3^{(2)} & \cdots & 0 \\ \vdots & \vdots & \ddots & \vdots \\ 0 & 0 & \cdots & A_3^{(D)} \end{bmatrix} \quad \mathbf{B}_{3v} = \begin{bmatrix} B_{3v}^{(1)} \\ B_{3v}^{(2)} \\ \vdots \\ B_{3v}^{(D)} \end{bmatrix} \quad \mathbf{B}_{3\omega} = \begin{bmatrix} B_{3\omega}^{(1)} \\ B_{3\omega}^{(2)} \\ \vdots \\ B_{3\omega}^{(D)} \end{bmatrix} \quad A_3^{(h)} = \begin{bmatrix} -R_{load}^{(h)}/L_{load}^{(h)} & \omega_{sys} \\ -\omega_{sys} & -R_{load}^{(h)}/L_{load}^{(h)} \end{bmatrix} B_{3\omega}^{(h)} = \begin{bmatrix} I_{3Q}^{(h)} \\ -I_{3D}^{(h)} \end{bmatrix}$$

E. System Stability Evaluation

The system stability is reflected by the eigenvalues of matrix $\mathbf{A}_{grid}$, which are determined by the characteristic equation $\det \Psi(\lambda) = 0$. The characteristic matrix $\Psi(\lambda)$ is given by

$$\Psi(\lambda) = \lambda I_0 - \mathbf{A}_{grid} \tag{55}$$

where I_0 is a $(14G + 2L + 2H) \times (14G + 2L + 2H)$ identity matrix. The eigenvalues are often referred to as modes, which reveal different frequency components in the system and the corresponding damping. If the real part of a mode is larger than zero, the system becomes unstable, and vice versa. The modes with smaller real parts are better damped in comparison to the modes with larger real parts.

V. Stability Analysis for Nonnegligible Communication Delay

With communication delay τ, the small-signal model of the microgrid is given by

$$\begin{bmatrix} \Delta\dot{\mathbf{x}}(t) \\ \Delta\mathbf{i}_{2DQ}(t) \\ \Delta\mathbf{i}_{3DQ}(t) \end{bmatrix} = \mathbf{A}_{grid-dr} \begin{bmatrix} \Delta\mathbf{x}(t) \\ \Delta\mathbf{i}_{2DQ}(t) \\ \Delta\mathbf{i}_{3DQ}(t) \end{bmatrix} + \mathbf{A}_{grid-sh} \begin{bmatrix} \Delta\mathbf{x}(t-\tau) \\ \Delta\mathbf{i}_{2DQ}(t-\tau) \\ \Delta\mathbf{i}_{3DQ}(t-\tau) \end{bmatrix}. \tag{56}$$

Note that the matrices $\mathbf{A}_{grid-dr}$ and $\mathbf{A}_{grid-sh}$ are readily obtained based on the decomposed model in the previous section. The system stability with respect to different modes is evaluated by solving the characteristic equation $\det \Omega(\lambda, \tau) = 0$ based on the characteristic matrix, given by

$$\Omega(\lambda, \tau) = \lambda I_0 - \mathbf{A}_{grid-dr} - \mathbf{A}_{grid-sh} e^{-\lambda\tau}. \tag{57}$$

It is worth mentioning that, as the communication delay τ approaches zero, we have the following property with respect to the characteristic matrix (57):

$$\begin{aligned} \lim_{\tau\to 0} \Omega(\lambda, \tau) &= \lim_{\tau\to 0} \left[\lambda I_0 - \mathbf{A}_{grid-dr} - \mathbf{A}_{grid-sh} e^{-\lambda\tau}\right] \\ &= \lambda I_0 - \mathbf{A}_{grid-dr} - \mathbf{A}_{grid-sh} \\ &= \lambda I_0 - \mathbf{A}_{grid} \\ &= \Psi(\lambda). \end{aligned} \tag{58}$$

In other words, the stability analysis reduces to the negligible communication delay case as $\tau \to 0$.

However, in comparison with the negligible communication delay case, the characteristic equation for the nonnegligible communication delay case has infinite number of roots since it is transcendental. Therefore, only a reduced set of roots can be obtained based on approximation. We adopt the method proposed in [20] based on the calculation of the eigenvalues of the following matrix

$$\Phi = \begin{bmatrix} \hat{\Theta} \otimes I_0 \\ \hline \mathbf{A}_{grid-sh} \ 0 \ \cdots \ 0 \ \mathbf{A}_{grid-dr} \end{bmatrix} \tag{59}$$

where $\otimes$ represents the Kroneckers product. Matrix $\hat{\Theta}$ consists of the first M rows of matrix $\Theta = -2D_M/\tau$, where $D_M = [d_M(i,j)]_{(M+1)\times(M+1)}$ is the Chebyshev's differentiation matrix of order M, given by

$$d_M(i,j) = \begin{cases} \frac{d_i(-1)^{i+j}}{d_j(\beta_{i-1}-\beta_{j-1})}, & \text{if } i \neq j \\ -\frac{1}{2}\frac{\beta_{i-1}}{1-\beta_{i-1}^2}, & \text{if } i = j \neq 1, M+1 \\ \frac{2N^2+1}{6}, & \text{if } i = j = 1 \\ -\frac{2N^2+1}{6}, & \text{if } i = j = M+1 \end{cases} \tag{60}$$

with $d_1 = d_{M+1} = 2$ and $d_2 = \cdots = d_M = 1$, and β_k $(k \in 0, 1, \cdots, M)$ given by

$$\beta_k = \cos\left(\frac{k\pi}{M}\right). \tag{61}$$

The value of M corresponds to the number of nodes for Chebyshev's discretization which determines the computational precision and complexity.

VI. Numerical Results

We use the droop control test system proposed in [5] as an example for performance evaluation. The microgrid consists of three generators, two lines, and two loads. The three generators have the same capacities and configurations. The desired sharing of the real and reactive power among the three generators are the same, i.e., $\alpha_P^{(g)} = \alpha_Q^{(g)} = \frac{1}{3}$ for $g \in \{1, 2, 3\}$. With traditional droop control strategy (or equivalently, the real power sharing gain $K_{P-sh}^{(g)} = 0$ and the reactive power sharing gain $K_{Q-sh}^{(g)} = 0$), the trace of the low-frequency modes which are sensitive to frequency and voltage droop gains is shown in Fig. 3. We can see that the low-frequency modes move towards two different directions as the frequency droop gain ($K_{P-dr}^{(g)}$) increases from 1×10^{-5} to 1.2×10^{-4}. Although some modes move towards the stable region with negative real parts, the other modes which are close to the imaginary axis move significantly towards the unstable region with positive real parts. On the other hand, the low-frequency modes move slightly towards the stable region as the voltage droop gain ($K_{Q-dr}^{(g)}$) increases. Although increasing the voltage droop gain can potentially improve microgrid stability, the low-frequency modes are generally less sensitive to the voltage droop gain than that to the frequency droop gain [5], which makes the stability enhancement less effective. Moreover, a change in the voltage droop gain may affect the sharing of reactive power among the DG units, which is not desired in microgrid operation. On the other hand, the information exchange based on a wireless network can

$$\mathbf{A}_{grid-dr} = \begin{bmatrix} [\mathbf{A}_{1-dr} + \mathbf{B}_1\mathbf{M}_1'\mathbf{R}_N\mathbf{M}_1\mathbf{C}_1] & [\mathbf{B}_1\mathbf{M}_1'\mathbf{R}_N\mathbf{M}_2] & [\mathbf{B}_1\mathbf{M}_1'\mathbf{R}_N\mathbf{M}_3] \\ [\mathbf{B}_{2v}\mathbf{R}_N\mathbf{M}_1\mathbf{C}_1 + \mathbf{B}_{2\omega}\mathbf{C}_{com-dr}] & [\mathbf{A}_2 + \mathbf{B}_{2v}\mathbf{R}_N\mathbf{M}_2] & [\mathbf{B}_{2v}\mathbf{R}_N\mathbf{M}_3] \\ [\mathbf{B}_{3v}\mathbf{R}_N\mathbf{M}_1\mathbf{C}_1 + \mathbf{B}_{3\omega}\mathbf{C}_{com-dr}] & [\mathbf{B}_{3v}\mathbf{R}_N\mathbf{M}_2] & [\mathbf{A}_3 + \mathbf{B}_{3v}\mathbf{R}_N\mathbf{M}_3] \end{bmatrix} \quad \mathbf{A}_{grid-sh} = \begin{bmatrix} [\mathbf{A}_{1-sh}] & 0 & \cdots & 0 \\ [\mathbf{B}_{2\omega}\mathbf{C}_{com-sh}] & \vdots & \ddots & \vdots \\ [\mathbf{B}_{3\omega}\mathbf{C}_{com-sh}] & 0 & \cdots & 0 \end{bmatrix}$$

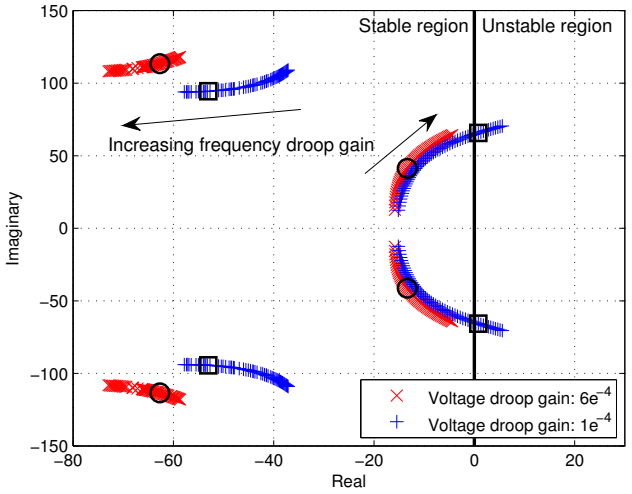

Fig. 3: Trace of low-frequency modes versus frequency and voltage droop gains for traditional droop control strategy.

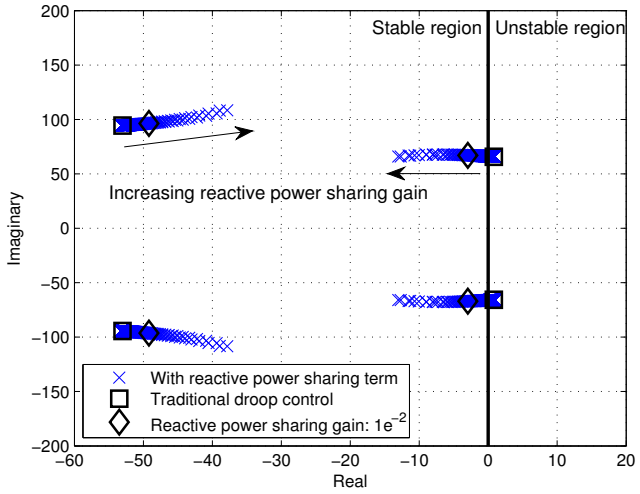

Fig. 5: Trace of low-frequency modes versus reactive power sharing gain.

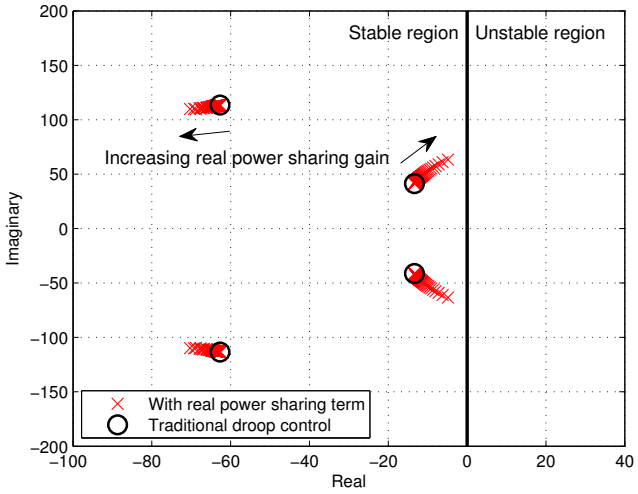

Fig. 4: Trace of low-frequency modes versus real power sharing gain.

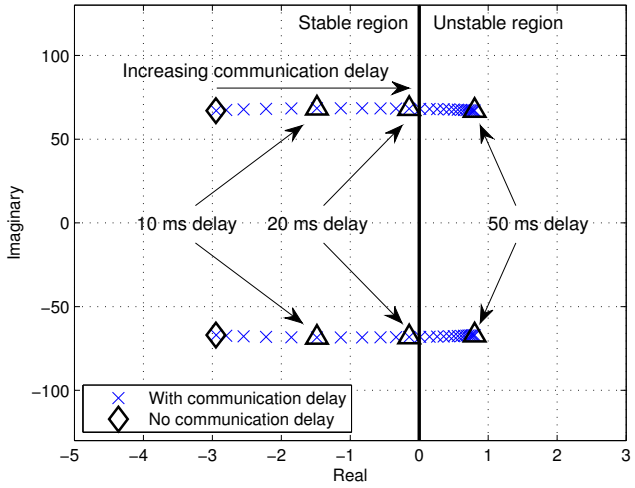

Fig. 6: Impact of communication delay on the locations of different modes.

potentially improve the microgrid stability. In the following performance evaluation, we use the modes marked by squares and circles in Fig. 3 (which correspond to frequency droop gains 1×10^{-4} and 5×10^{-5}, respectively) as reference points.

Fig. 4 demonstrates the impact of real power sharing gain. The reactive power sharing gain is zero. The frequency and voltage droop gains of the reference points with respect to the traditional droop control strategy are given by 5×10^{-5} and 6×10^{-4}, respectively, while the corresponding modes are marked by circles in Fig. 3. Similar to the change in frequency droop gain, the low-frequency modes move towards two different directions as the real power sharing gain increases (from 0 to 6.7×10^{-5}). Since some of the modes which are close to the imaginary axis move slightly towards the unstable region, the stability improvement by adjusting the real power sharing gain is not obvious, mainly because the real power sharing based on traditional droop control is already accurate in microgrid operation [9].

Next, we fix the real power sharing gain to zero (the corresponding modes are marked by squares in Fig. 3) and investigate the impact of reactive power sharing gain. Note that the original microgrid is unstable since the modes marked by squares in Fig. 3 are in the unstable region. The impact of reactive power sharing gain is shown in Fig. 5. We observe that the low-frequency modes which are in the unstable region move towards the stable region as the reactive power sharing gain increases (from 0 to 0.1) such that the microgrid can be stabilized. The reason is that, the information provided by the wireless network can correct the reactive power sharing error based on an additional integral control term [12]. According to traditional droop control strategy, the inverters at different locations of microgrid share different amount of reactive power as the load changes significantly, due to the fact that the line impedance is not negligible. This is also known as one of the

major limitations of traditional droop control in microgrid [5]. On the other hand, by sharing the reactive power among the DG units evenly, the temporary overloading of DG units can be avoided and the microgrid stability can be improved based on our proposed control strategy.

From Fig. 4 and Fig. 5, we see that the proposed control strategy can improve system stability (especially by adjusting the reactive power sharing gain) given that the communication delay is negligible. To investigate how the communication delay can affect the system stability, the trace of the modes when communication delay increases from 0 to 50 ms is shown in Fig. 6. We choose $M = 2$ for the Chebyshev's discretization [20]. The frequency droop gain, voltage droop gain, real power sharing gain, and reactive power sharing gain are set to 1×10^{-4}, 1×10^{-4}, 0, and 1×10^{-2}, respectively. The reference points with respect to the performance without communication delay are marked by diamonds in Fig. 5 and Fig. 6, respectively. We only show the low-frequency modes which are close to the imaginary axis since these modes dominate the system stability as the communication delay changes. We can see that the low-frequency modes move towards the unstable region as the communication delay increases. The system becomes unstable again when the communication delay is large (i.e., more than 20 ms for the microgrid under consideration). How to mitigate the negative effect of communication delay to further improve system stability needs further study.

VII. Conclusions

In this paper, we investigate the stability enhancement of decentralized inverter control in distributed generation microgrids. A wireless network is established to acquire the information of total real and reactive power generation of all DG units. A power sharing based control strategy is proposed, which introduces additional terms to the traditional droop control strategy to capture the differences between the desired and actual real and reactive power generation. An analytical model is developed to evaluate the small-signal stability of the microgrid under our proposed control strategy. Numerical results indicate that, our proposed control strategy can improve the system stability when the communication delay is small.

Future work includes the communication delay reduction based on communication protocol design, and the voltage stability improvement while maintaining an accurate reactive power sharing among the DG units. Moreover, how to improve microgrid stability under packet losses in multiagent coordination over an unreliable wireless channel [21] is critical but needs further investigation.

References

[1] H. Liang, B. J. Choi, W. Zhuang, and X. Shen, "Decentralized inverter control in microgrids based on power sharing information through wireless communications," in *Proc. IEEE GLOBECOM'12*, Dec. 2012.

[2] S. Chowdhury, S. P. Chowdhury, and P. Crossley, *Microgrids and Active Distribution Networks*. Institution of Engineering and Technology, 2009.

[3] H. Farhangi, "The path of the smart grid," *IEEE Power and Energ. Mag.*, vol. 8, no. 1, pp. 18–28, Jan.-Feb. 2010.

[4] Y. Mohamed and E. F. El-Saadany, "Adaptive decentralized droop controller to preserve power sharing stability of paralleled inverters in distributed generation microgrids," *IEEE Trans. Power Electron.*, vol. 23, no. 6, pp. 2806–2816, Nov. 2008.

[5] N. Pogaku, M. Prodanovic, and T. C. Green, "Modeling, analysis and testing of autonomous operation of an inverter-based microgrid," *IEEE Trans. Power Electron.*, vol. 22, no. 2, pp. 613–625, Mar. 2007.

[6] J. M. Guerrero, J. Matas, L. G. Vicuna, M. Castilla, and J. Miret, "Decentralized control for parallel operation of distributed generation inverters using resistive output impedance," *IEEE Trans. Ind. Electron.*, vol. 54, no. 2, pp. 994–1004, Apr. 2007.

[7] C. K. Sao and P. W. Lehn, "Control and power management of converter fed microgrids," *IEEE Trans. Ind. Electron.*, vol. 23, no. 3, pp. 1088-1098, Aug. 2008.

[8] Y. W. Li and C. N. Kao, "An accurate power control strategy for power-electronics-interfaced distributed generation units operating in a low-voltage multibus microgrid," *IEEE Trans. Power Electron.*, vol. 24, no. 12, pp. 2977–2988, Dec. 2009.

[9] Y. Li and Y. Li, "Power management of inverter interfaced autonomous microgrid based on virtual frequency-voltage frame," *IEEE Trans. Smart Grid*, vol. 2, no. 1, pp. 30–40, Mar. 2011.

[10] H. Liang, B. J. Choi, A. Abdrabou, W. Zhuang, and X. Shen, "Decentralized economic dispatch in microgrids via heterogeneous wireless networks," *IEEE J. Sel. Areas Commun.*, vol. 30, no. 6, pp. 1061–1074, Jul. 2012.

[11] J. M. Undrill, "Dynamic stability calculations for an arbitrary number of interconnected synchronous machines, *IEEE Trans. Power Apparat. Syst.*, vol. PAS-87, no. 3, pp. 835–845, Mar. 1968.

[12] J. He and Y. W. Li, "An accurate reactive power sharing control strategy for DG units in a microgrid," in *Proc. PICPE and ECCE'11*, pp. 551–556, May-Jun., 2011.

[13] S. Galli, A. Scaglione, and Z. Wang, "For the grid and through the grid: the role of power line communications in the smart grid," *Proc. IEEE*, vol. 99, no. 6, pp. 998–1027, Jun. 2011.

[14] Y. Xu and W. Liu, "Novel multiagent based load restoration algorithm for microgrids," *IEEE Trans. Smart Grid*, vol. 2, no. 1, pp. 152–161, Mar. 2011.

[15] H. Liang, A. Abdrabou, B. J. Choi, W. Zhuang, X. Shen, and A. S. A. Awad, "Multiagent coordination in microgrids via wireless networks," *IEEE Wireless Commun.*, vol. 19, no. 3, pp. 14–22, Jun. 2012.

[16] L. Xiao and S. Boyd, "Fast linear iterations for distributed averaging," in *Proc. IEEE CDC'03*, vol. 5, pp. 4997–5002, Dec. 2003.

[17] R. Olfati-Saber, J. Fax, and R. Murray, "Consensus and cooperation in networked multi-node systems," *Proc. IEEE*, vol. 95, pp. 215–233, Jan. 2007.

[18] B. J. Choi, H. Liang, X. Shen, and W. Zhuang, "DCS: distributed asynchronous clock synchronization in delay tolerant networks," *IEEE Trans. Parallel Distrib.*, vol. 23, no. 3, pp. 491–504, Mar. 2012.

[19] P. Kundur, J. Paserba, V. Ajjarapu, G. Andersson, A. Bose, C. Canizares, N. Hatziargyriou, D. Hill, A. Stankovic, C. Taylor, T. Van Cutsem, and V. Vittal, "Definition and classification of power system stability IEEE/CIGRE joint task force on stability terms and definitions," *IEEE Trans. Power Syst.*, vol. 19, no. 3, pp. 1387–1401, Aug. 2004.

[20] F. Milano and M. Anghel, "Impact of time delays on power system stability," *IEEE Trans. Circ. Syst. I*, vol. 59, no. 3, pp. 1–12, Mar. 2012.

[21] T. C. Aysal, M. E. Yildiz, A. D. Sarwate, and A. Scaglione, "Broadcast gossip algorithms for consensus," *IEEE Trans. Signal Process.*, vol. 57, no. 7, pp. 2748–2761, Jul. 2009.

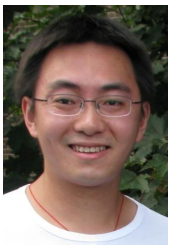

Hao Liang (S'09) is currently working toward a Ph.D. degree at the Department of Electrical and Computer Engineering, University of Waterloo, Canada. His research interests are in the areas of wireless communications, wireless networking, and smart grid. He is a recipient of the Best Student Paper Award from IEEE 72nd Vehicular Technology Conference (IEEE VTC Fall-2010), Ottawa, ON, Canada. He received the Chinese Government Award for Outstanding Self-Financed Students Abroad in 2011. He served as the Technical Program Committee (TPC) Member for 2012 IEEE International Conference on Power and Energy (IEEE PECON 2012), IEEE VTC Fall-2011, and IEEE VTC Fall-2010. He has been serving as the System Administrator of IEEE Transactions on Vehicular Technology since 2009.

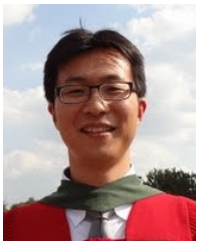

Bong Jun Choi (M'11) received the B.Sc. (2003) and M.Sc. (2005) degrees from Yonsei University, Republic of Korea, both in electrical and electronics engineering, and the Ph.D. (2011) degree from University of Waterloo, Canada, in electrical and computer engineering. He is an assistant professor at the Department of Computer Science, State University of New York Korea. He was a software engineer at Telecommunication Network Division of Samsung Electronics in 2005-2006. He was a postdoctoral research fellow at the Department of Electrical and Computer Engineering, University of Waterloo in 2011-2012. His current research focuses on energy efficiency, distributed computing, and medium access control in wireless communications, mobile wireless networks, and smart grid. He serves as an editor of KSII Transactions on Internet and Information Systems. He is a member of the IEEE and the ACM.

Weihua Zhuang (F'08) has been with the Department of Electrical and Computer Engineering, University of Waterloo, Canada, since 1993, where she is a Professor and a Tier I Canada Research Chair in Wireless Communication Networks. Her current research focuses on resource allocation and QoS provisioning in wireless networks. Dr. Zhuang is a co-recipient of the Best Paper Awards from the IEEE International Conference on Communications (ICC) 2012 and 2007, IEEE Multimedia Communications Technical Committee in 2011, IEEE Vehicular Technology Conference (VTC) Fall 2010, IEEE Wireless Communications and Networking Conference (WCNC) 2010 and 2007, and the International Conference on Heterogeneous Networking for Quality, Reliability, Security and Robustness (QShine) 2008 and 2007. She received the Outstanding Performance Award 4 times since 2005 from the University of Waterloo, and the Premier's Research Excellence Award in 2001 from the Ontario Government. Dr. Zhuang is the Editor-in-Chief of IEEE Transactions on Vehicular Technology, and the Technical Program Symposia Chair of the IEEE Globecom 2011. She is a Fellow of the IEEE, a Fellow of the Canadian Academy of Engineering (CAE), a Fellow of the Engineering Institute of Canada (EIC), and an IEEE Communications Society Distinguished Lecturer (2008-2011).

Xuemin (Sherman) Shen (M'97-SM'02-F'09) received the B.Sc.(1982) degree from Dalian Maritime University (China) and the M.Sc. (1987) and Ph.D. degrees (1990) from Rutgers University, New Jersey (USA), all in electrical engineering. He is a Professor and University Research Chair, Department of Electrical and Computer Engineering, University of Waterloo, Canada. He was the Associate Chair for Graduate Studies from 2004 to 2008. Dr. Shen's research focuses on resource management in interconnected wireless/wired networks, wireless network security, wireless body area networks, vehicular ad hoc and sensor networks. He is a co-author/editor of six books, and has published more than 600 papers and book chapters in wireless communications and networks, control and filtering. Dr. Shen served as the Technical Program Committee Chair for IEEE VTC'10 Fall, the Symposia Chair for IEEE ICC'10, the Tutorial Chair for IEEE VTC'11 Spring and IEEE ICC'08, the Technical Program Committee Chair for IEEE Globecom'07, the General Co-Chair for Chinacom'07 and QShine'06, the Chair for IEEE Communications Society Technical Committee on Wireless Communications, and P2P Communications and Networking. He also serves/served as the Editor-in-Chief for IEEE Network, Peer-to-Peer Networking and Application, and IET Communications; a Founding Area Editor for IEEE Transactions on Wireless Communications; an Associate Editor for IEEE Transactions on Vehicular Technology, Computer Networks, and ACM/Wireless Networks, etc.; and the Guest Editor for IEEE JSAC, IEEE Wireless Communications, IEEE Communications Magazine, and ACM Mobile Networks and Applications, etc. Dr. Shen received the Excellent Graduate Supervision Award in 2006, and the Outstanding Performance Award in 2004, 2007 and 2010 from the University of Waterloo, the Premier's Research Excellence Award (PREA) in 2003 from the Province of Ontario, Canada, and the Distinguished Performance Award in 2002 and 2007 from the Faculty of Engineering, University of Waterloo. Dr. Shen is a registered Professional Engineer of Ontario, Canada, an IEEE Fellow, an Engineering Institute of Canada Fellow, a Canadian Academy of Engineering Fellow, and a Distinguished Lecturer of IEEE Vehicular Technology Society and Communications Society.